Photodissociation of Methyl Nitrate in a Molecular Beam

Xuefeng Yang, Peter Felder, and J. Robert Huber*

Physikalisch-Chemisches Institut der Universität Zürich, Winterthurerstrasse 190,
CH-8057 Zürich, Switzerland

Received: June 15, 1993; In Final Form: August 9, 1993®

The photodissociation of methyl nitrate, CH_3ONO_2, has been investigated by photofragment translational spectroscopy. At the photolysis wavelength of 193 nm the predominant primary decay (~70%) involves the fission of the weak CH_3O-NO_2 bond ($D_0^{I} \sim 41$ kcal/mol) to yield $CH_3O + NO_2$ fragment pairs which show a bimodal translational energy distribution. The component consisting of the fast fragment pairs has an average translational energy $\langle E_T \rangle = 41$ kcal/mol and a recoil anistropy $\beta = 0.9$, while the slow component is characterized by $\langle E_T \rangle = 19$ kcal/mol and $\beta = 0$. A significant portion of the NO_2 fragments of the slow component is subject to a unimolecular decay to NO + $O(^3P)$. An additional primary decay route leads to the formation of methyl nitrite, CH_3ONO, and atomic oxygen $O(^1D)$ with $\langle E_T \rangle = 6$ kcal/mol and $\beta = 1.2$. This competing reaction requires fission of the strong N–O bond ($D_0^{II} \sim 118$ kcal/mol) and its occurrence indicates an initial localization of the photoexcitation on the NO_2 moiety in the parent molecule. At higher laser fluence secondary photodissociation of the primary fragments CH_3ONO was observed. Photolysis at 248 nm is shown to produce $CH_3O + NO_2$ fragment pairs exclusively, with $\langle E_T \rangle = 17$ kcal/mol.

I. Introduction

Nitric oxide (NO) and nitrogen dioxide (NO_2), collectively denoted as NO_x, play a central role in the catalytic and photochemical processes of the atmosphere.[1-3] The most important precursor and product species of atmospheric NO_x are nitric acid (HNO_3), nitrate ion (NO_3^-) in aerosols, and peroxyacetic nitric anhydride (PAN). These compounds and NO_x account for most of what is often referred to as reactive odd-nitrogen, NO_y. Recent atmospheric measurements[3,4] indicate that in some cases 7–42% of the NO_y consists of relatively stable organic species, most notably the alkyl nitrates $RONO_2$, R = CH_3, C_2H_5, etc. These compounds are formed as minor products in the reaction of organic peroxy radicals with NO and are removed both by reaction with OH radicals and by photolysis with light in the near-UV region. The relative importance of the two destruction mechanisms depends on the atmospheric conditions and on the substituent group R, with the photolytic decay route being most important in the case of methyl nitrate, CH_3ONO_2.[3] From this point of view the photodissociation mechanism of alkyl nitrates merits attention.

The UV spectrum of methyl nitrate exhibits a weak and broad absorption band with a maximum around 260 nm (σ(260 nm) $\sim 2 \times 10^{-20}$ cm^2) followed by a stronger band in the region of 190 nm (σ(193 nm) $\sim 2 \times 10^{-17}$ cm^2).[3,5] The corresponding electronic transitions have been attributed to $\pi^* \leftarrow n$ and $\pi^* \leftarrow \pi$ excitations, respectively, which are localized on the NO_2 moiety.[6] The broad and unstructured absorption features of CH_3ONO_2 are an indication of rapid photodissociation. On the basis of an assumed photodissociation quantum yield of unity and the best estimates of the pertinent bimolecular reaction rates, the average residence time of a methyl nitrate molecule in the atmosphere has been calculated for various atmospheric conditions[3,5] to be on the order of 1 day.

Early pyrolysis[7] and UV flash photolysis[8] experiments in the gas phase have shown that the predominant primary dissociation process of CH_3ONO_2 produces CH_3O and NO_2 fragments. This result was obtained from the analysis of final products in the bulk phase, but no direct measurements concerning identity and energy contents of *nascent* photofragments of methyl nitrate have been reported so far. To measure the translational and internal energy disposal of the dissociation products under collisionless conditions we have studied methyl nitrate at 193 and 248 nm using the technique of photofragment translational spectroscopy (PTS).[9-11] This method is ideally suited for the investigation of primary and secondary dissociation processes and has been extensively applied to disentangle the competing dissociation pathways in polyatomic molecules such as acrolein and propynal,[12] thionyl chloride,[13] thiirane,[14] ClNO,[15] allene,[16] CH_3SH,[17] and $ClONO_2$.[18]

In the case of methyl nitrate photolysis at 193 nm (148 kcal/mol) the following reactions are energetically accessible:

$$CH_3ONO_2(\tilde{X}^1A') \rightarrow CH_3O(\tilde{X}^2E) + NO_2(\tilde{X}^2A_1) \qquad \Delta H^\circ = 41 \text{ kcal/mol} \qquad (1)$$

$$CH_3ONO_2(\tilde{X}^1A') \rightarrow CH_3ONO(\tilde{X}^1A') + O(^1D) \qquad \Delta H^\circ = 118 \text{ kcal/mol} \qquad (2)$$

$$CH_3ONO_2(\tilde{X}^1A') \rightarrow CH_3(\tilde{X}^2A''_2) + NO_3(\tilde{X}^2A'_2) \qquad \Delta H^\circ = 83 \text{ kcal/mol} \qquad (3)$$

The dissociation energies quoted here and shown in the energy level diagram of Figure 1 have been derived from tabulated thermochemical data.[19-21] In reaction 1, either the CH_3O or the NO_2 fragment can also be formed in one of the electronically excited states ($\tilde{A}^2A_1$ for CH_3O; $\tilde{A}^2B_2$, $\tilde{B}^2B_1$ and $\tilde{C}^2A_2$ for NO_2). Reaction 2, although energetically unfavorable, should be taken into consideration since the analogous process has been reported to occur in the photolysis of ethyl nitrate[22] with a quantum yield of 0.139. Here, the formation of ground-state oxygen atoms $O(^3P)$ would reduce the endothermicity of reaction 2 by 45.4 kcal/mol[20] but the process would be spin-forbidden. Reaction 3, on the other hand, is interesting in view of the well-established importance of NO_3 as a tropospheric species at night time.[21,23] Finally, it should be mentioned that in the case of $ClONO_2$, a molecule that is structurally similar to CH_3ONO_2, the PTS technique has provided unambiguous evidence for the occurrence of the reactions corresponding to processes 1 and 3 as competing primary decay steps.[18]

While the large absorption cross section of CH_3ONO_2 at 193 nm allows us to study the photodissociation in considerable detail, the tropospherically relevant photolysis occurs at longer wave-

---

® Abstract published in *Advance ACS Abstracts,* October 1, 1993.

0022-3654/93/2097-10903$04.00/0

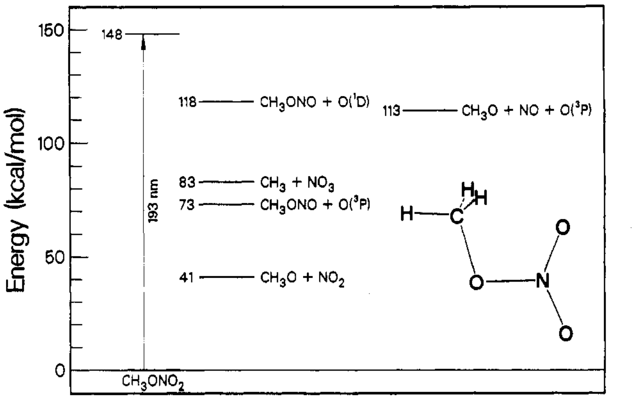

Figure 1. Energy level diagram for the photofragmentation of CH_3ONO_2 at 193 nm. The insert shows the geometry of the parent molecule in the electronic ground state.[38]

length (λ > 280 nm) where the absorption cross section is very small.[3,5] To investigate the photodissociation in this absorption band region, we have carried out a series of PTS measurements with a KrF laser at 248 nm (115 kcal/mol). Since at this excitation energy, reaction 2 is not accessible, one expects reaction 1 to be the major dissociation pathway, with possible competition of the C–O bond-fission process 3.

II. Experimental Section

The crossed laser–molecular beam apparatus consists of a pulsed rotatable molecular beam source and a spatially fixed quadrupole mass spectrometer as detector.[24] The pulsed laser beam is directed along the rotation axis of the molecular beam source and the variable scattering angle Θ is given by the direction of the molecular beam and the detector axis. The 193.3-nm laser pulses are generated by an ArF excimer laser (Lambda Physik EMG101). After a flight path of 34.5 cm, the photofragments are ionized by electron bombardment, discriminated according to their mass-to-charge ratio (m/e) in a quadrupole mass filter and detected by an electron multiplier. The time-of-flight (TOF) distributions of the fragments are recorded with a multichannel scaler. An offset of $3.9(m/e)^{1/2}$ μs due to the transit time of the ions through the mass filter has been subtracted in all the TOF spectra shown in the sections below. The power dependence of the photofragment signals at 193 nm was studied by means of a variable attenuation plate (Laseroptik GmbH, Garbsen, Germany) which provides laser pulse energies between 3 and 30 mJ corresponding to a fluence at the beam intersection of 50 and 500 mJ/cm^2, respectively. The photofragment recoil anisotropy was obtained by recording the TOF distributions from a linearly polarized (polarization degree 92%) photolysis laser and by changing the polarization angle ϵ (defined as the angle between the electric vector of the laser beam and the detection axis) through a 180° range with a half-wave plate. The experiments at 248 nm were carried out with an unpolarized KrF laser at a fluence of 1.5 J/cm^2.

Methyl nitrate was prepared according to a published procedure[25] and purified by several freeze–pump–thaw cycles. To minimize the explosion hazard, only very small samples of the compound were handled at a given time. In general, a gas mixture of methyl nitrate in helium was prepared in a stainless steel vessel and admitted to the pulsed valve through a pressure regulating system. The molecular beam velocity distribution was determined by the laser-induced hole burning method.[26] Most of the TOF spectra were obtained with 4% CH_3ONO_2 in He at a total stagnation pressure of 200 mbar yielding a beam with a most probable velocity $v_0 = 1200$ m/s and a full width at half-maximum of 145 m/s as based on a least squares fit to the density distribution $f(v) = C \exp[-(v - v_0)^2/\alpha^2]$, where $\alpha = 88$ m/s.

III. Results and Analysis

III.1. General Remarks. Since most of the experiments were performed with a photolysis wavelength of 193 nm, the results obtained at 248 nm are presented separately in section III.5. Photofragment signals were detected at m/e = 15, 16, 29, 30, 46, and 60. The result of the analysis of the TOF and angular fragment distributions led us to conclude that photodissociation of methyl nitrate at 193 nm proceeds via two competing and chemically distinct primary decay channels:

$$\begin{array}{lccccr} CH_3ONO_2 \xrightarrow{h\nu} & CH_3O & + & NO_2 & & \text{(I)} \\ & m/e = 29, 15 & & m/e = 46, 30 & & \\ \xrightarrow{h\nu} & CH_3ONO & + & O & & \text{(II)} \\ & m/e = 60, 46, 30, 29, 15 & & m/e = 16 & & \end{array}$$

(The mass-to-charge ratio, m/e, at which the signal was observed is indicated below the formula.)

Difficulties in establishing the above reaction scheme arose because fragmentation of reaction products in the electron bombardment ionizer prevented the detection of CH_3O and CH_3ONO at their parent ion masses of 31 and 61, respectively. However, the identification of the dissociation products was achieved by exploiting the conservation of linear momentum which implies a strict correlation between the recoil velocities of the members of each photofragment pair. This will become evident when the individual TOF distributions are presented. A further difficulty encountered in the initial experiments was the formation of methyl nitrate clusters. Photodissociation of the clusters produced a particularly strong signal in the TOF spectrum at m/e = 46, but optimization of the beam conditions with respect to stagnation pressure and methyl nitrate concentration allowed us to effectively suppress cluster formation. Hence, the TOF spectra shown below are exclusively due to the photodissociation of monomeric methyl nitrate.

The total translational energy distributions $P(E_T)$ of the photofragment pairs were obtained with a forward convolution method[27] that transforms the center-of-mass (CM) to the laboratory (LAB) frame by taking into account the broadening effects arising from the velocity spread of the parent beam, the finite length of the ionizer, and the size of the laser beam focus. In Figures 2 and 3 the best-fitting TOF distributions are displayed as thick solid lines.

The reaction enthalpies ΔH_{rxn} of the pertinent dissociation processes are displayed in Figure 1 and listed in Table I together with the energies that are available to the photodissociation products

$$E_{avl} = h\nu - \Delta H_{rxn} \qquad (4)$$

where $h\nu$ refers to the photon energy and where the internal energy of the parent molecule could be neglected owing to the cold supersonic beam conditions. Also listed in Table I are the average translational energies determined from the experimental data.

The angular distribution of the photofragments in the CM frame is given by $w(\theta) \propto 1 + \beta P_2(\cos\theta)$, where P_2 is the second-order Legendre polynomial and θ is the angle between the electric vector of the laser light and the CM fragment recoil direction.[28] The anisotropy parameters β of the different dissociation channels were derived from the relative intensities of the TOF signals at various angles ϵ taken with a polarized photolysis laser.

III.2. Recoil Distributions. We first consider the results obtained with the unpolarized photolysis laser. The TOF spectra at m/e = 29 (CHO^+) recorded with LAB scattering angles Θ = 21° and 36° are displayed in Figure 2. Three distinct signal components are evident at Θ = 21° which have been labeled as A, B, and C in order of decreasing recoil velocity. Due to the

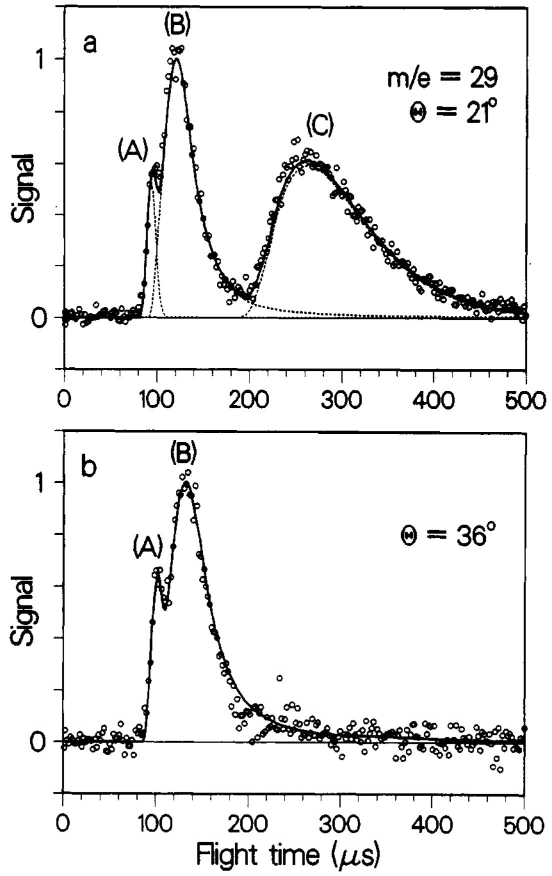

Figure 2. Photodissociation of CH_3ONO_2 at 193 nm. TOF distributions measured at $m/e = 29$ with $\Theta = 21°$ (a) and 36° (b). Circles denote the experimental data. The solid line represents the best fit calculated with the $P(E_T)$ distributions shown in Figure 4b (peaks A and B, $CH_3O + NO_2$ channel) and Figure 4a (peak C, $CH_3ONO + O(^1D)$ channel). The dashed lines indicate the three components, respectively.

low recoil velocity, the signal from component C is not discernible at the larger scattering angle $\Theta = 36°$. Signals A and B are both attributed to the CH_3O radicals formed in reaction I whereas peak C is assigned to CH_3ONO produced in reaction II due to the fact that peak C is also observed at $m/e = 15$ (CH_3^+), 30 (NO^+), 46 (NO_2^+), and 60 (CH_2ONO^+), as shown in Figure 3. The relative intensity of component C in the TOF spectra recorded at various m/e ratios is in close agreement with the fragmentation pattern of CH_3ONO measured in a control experiment using the same ionizer conditions. Moreover, the anisotropy parameters measured at $m/e = 29$ and 60 for component C agree within experimental error (see below). The TOF distribution at $m/e = 60$ was used to calculate the $P(E_T)$ distribution of reaction II which is reproduced in Figure 4a and which provides an excellent fit to the slow peak C in the TOF spectra at $m/e = 60$, 46, 30, and 15.

The assignment of peak A in the TOF spectrum at $m/e = 29$ (see Figure 2) as being due to the CH_3O fragments from reaction I is confirmed by the observation of the momentum-matched signal of the NO_2 fragments at $m/e = 46$ (see Figure 3b). The second TOF peak B observed at $m/e = 29$, albeit showing no obvious "partner" signal at $m/e = 46$ is, nevertheless, definitively assigned to CH_3O photofragments for the following reasoning. While, in principle, the CHO^+ ions could also originate from CH_2O or CHO formed in a different photodissociation process, this possibility can be ruled out by the close similarity of the TOF signals at $m/e = 29$ (CHO^+) and 15 (CH_3^+), implying peak B to originate from a species that contains the CH_3O moiety. CH_3ONO, however, is excluded since it would produce a readily detectable signal at $m/e = 46$, whereas CH_3OO and CH_3ON, formed in a hypothetical elimination of NO or O_2, would necessarily have a longer flight time. Therefore, we conclude that peak B at $m/e = 29$ is due to CH_3O fragments formed in coincidence with internally hot and unstable NO_2. The $P(E_T)$ distributions displayed in Figure 4b were derived from the TOF data taken at $m/e = 29$ using the different anisotropies of signals A and B (see below) to separate the corresponding contributions. The average translational energies of the fragments represented by peaks A, B, and C are 41, 19, and 6 kcal/mol, respectively.

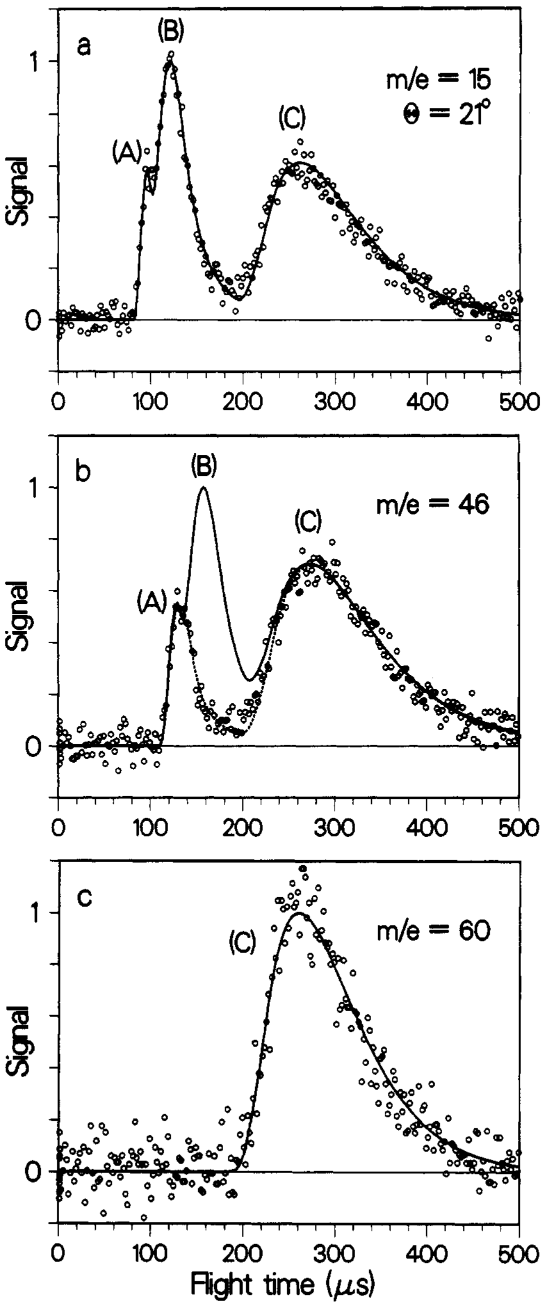

Figure 3. Photodissociation of CH_3ONO_2 at 193 nm. TOF distributions measured at $m/e = 15$ (a), 46 (b) and 60 (c) with $\Theta = 21°$. The symbols A, B, and C have the same meaning as in Figure 2. The solid line in (b) was calculated with the $P(E_T)$ distributions of Figure 4, whereas the dashed line in (b) was calculated using the *modified* energy distribution shown as *dashed* curve in Figure 4b; see text.

TABLE I. Photodissociation of Methyl Nitrate at 193 nm[a]

reaction	dissociation product	dissociation pathway	rel yield	E_{avl}	E_T^{max}	$\langle E_T \rangle$	$\langle E_{int} \rangle$	β
(I)	$CH_3O + NO_2$	IA	0.1	107	56	41	66	+0.9
		IB	0.6		40	19	88	0
(II)	$CH_3ONO + O(^1D)$		0.3	30	26	6	24	+1.2

[a] All energy values listed are in kcal/mol.

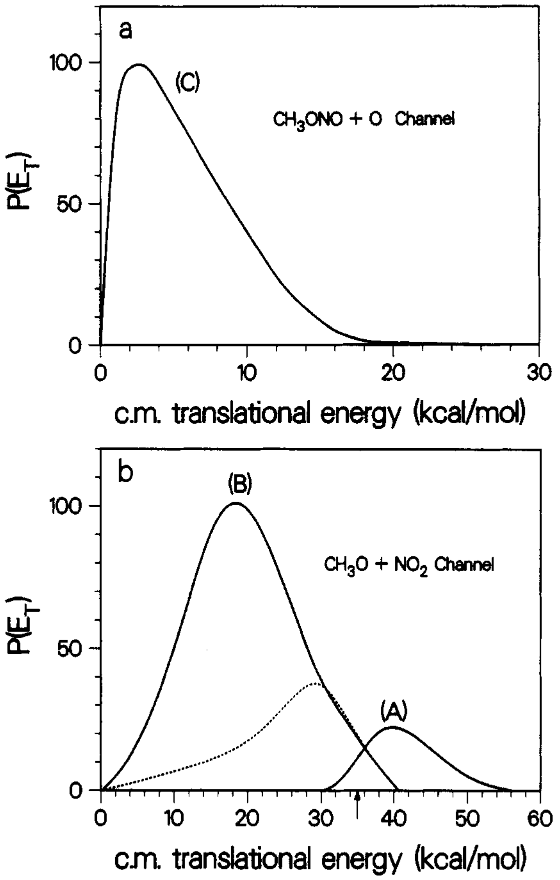

Figure 4. Center-of-mass translational energy distribution $P(E_T)$ of the fragments from the photodissociation of CH_3ONO_2 at 193 nm. (a) CH_3ONO + $O(^1D)$ channel, corresponding to peak C in the TOF distributions. (b) $CH_3O + NO_2$ channel, corresponding to peaks A and B in the TOF distributions. The *dashed* line within peak B is the $P(E_T)$ which fits the corresponding peak of the TOF distribution at $m/e = 46$ and thus pertains to *stable* NO_2 fragments.

To achieve a satisfactory fit of the data at $m/e = 46$ the component B of $P(E_T)$ was reduced by about 70% on the low energy side, as indicated by the dotted line in Figure 4b. This dotted curve represents the energy distribution of CH_3O fragments formed with a *stable* NO_2 partner, an interpretation supported by the fact that the dotted and solid curves in Figure 4b start to separate at $E_T \sim 32$ kcal/mol, which is slightly below the threshold kinetic energy for secondary dissociation of NO_2 to NO + $O(^3P)$. This threshold energy is calculated to be 35 kcal/mol by subtracting the accurately known dissociation energy $D_0(NO_2)$ = 71.8 kcal/mol[29] from the available energy of reaction I, E_{avl} = 107 kcal/mol (see Table I). The $P(E_T)$ distributions used to fit peaks A, B, and C at $m/e = 29$ were found also to reproduce the TOF spectrum at $m/e = 15$, implying the CH_3^+ ions originate from the CH_3O and CH_3ONO fragments cracked in the ionizer. Since no additional peak attributable to the methyl radicals produced in reaction 3 was observed at $m/e = 15$, we can safely conclude that the formation of $CH_3 + NO_3$ is not an important primary process.

The angular distribution of the photofragments was determined from the TOF distributions measured at $m/e = 29$ with the beam source angle $\Theta = 21°$ and the laser polarization angles $\epsilon = -20°$, 25°, 70°, and 115°. The anisotropy parameters of the three signal components were obtained as follows. First, the angular dependence of the integrated signal of peak C was used to determine the anisotropy parameter $\beta(C) = 1.2 \pm 0.1$, where the averaging effects caused by incomplete laser polarization and molecular beam velocity distribution were carefully taken into account. Figure 5a exhibits the best fit of the angular distribution. Subsequently, the anisotropy parameters $\beta(A) = 0.9 \pm 0.1$ and $\beta(B) = 0 \pm 0.1$ were found iteratively by requiring that the *relative* intensities of the TOF peaks A and B (calculated with the forward convolution method[27]) match those of the experimental polarized TOF spectra, measured at $\Theta = 21°$ (with four polarization angles ϵ) and at $\Theta = 36°$ (with 2 polarization angles ϵ). The resulting fits obtained at $\Theta = 36°$ are displayed in Figure 5b,c. It is important to note that polarization measurements carried out at $m/e = 60$, where only component C is present, are consistent with $\beta(C) = 1.2$ derived from the TOF data at $m/e = 29$. Consequently, since the photodissociation of methyl nitrate *clusters* was found to give rise to a slow TOF signal with an *isotropic* recoil distribution, these observations strongly support our assignment of decay channel C as being due to the formation of $CH_3ONO + O(^1D)$ and not to photodissociation products of methyl nitrate clusters.

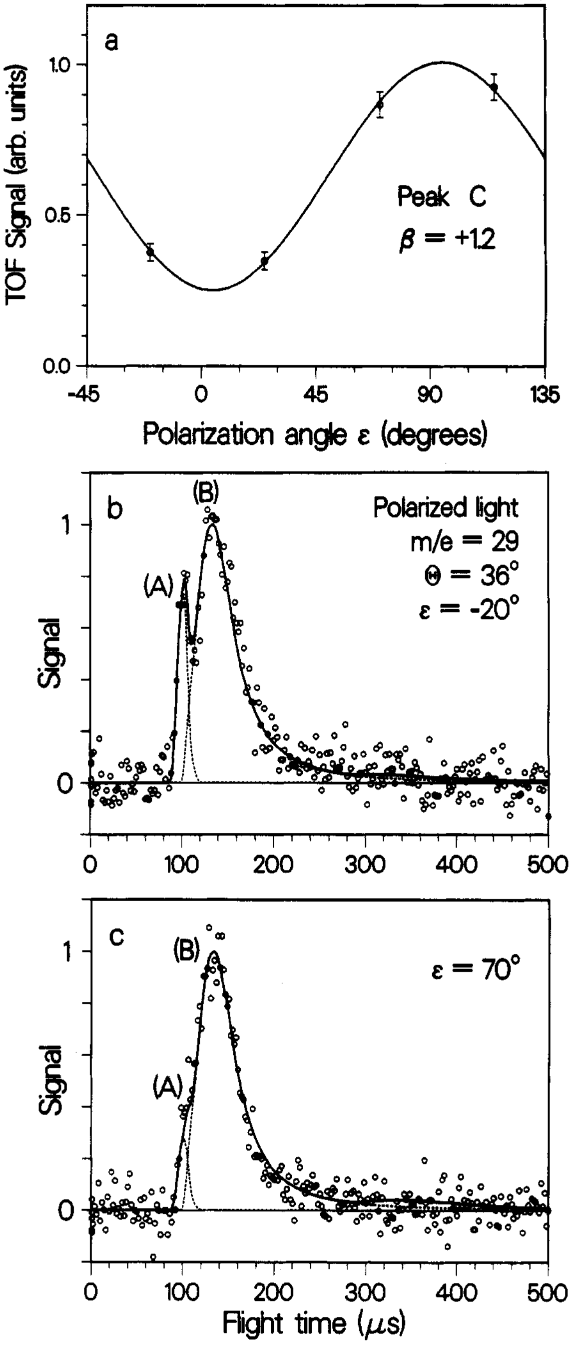

Figure 5. Photodissociation of CH_3ONO_2 at 193 nm using polarized laser light. (a) Angular distributions of peak C measured at $m/e = 29$ and $\Theta = 21°$. (b) and (c) TOF distributions measured at $m/e = 29$ with $\Theta = 36°$ and a polarization angle $\epsilon = -20°$ and +70°, respectively.

III.3. Branching Ratios. Having established the $P(E_T)$ distributions and β parameters we proceed to assess the relative importance of the primary dissociation channels. If one knows

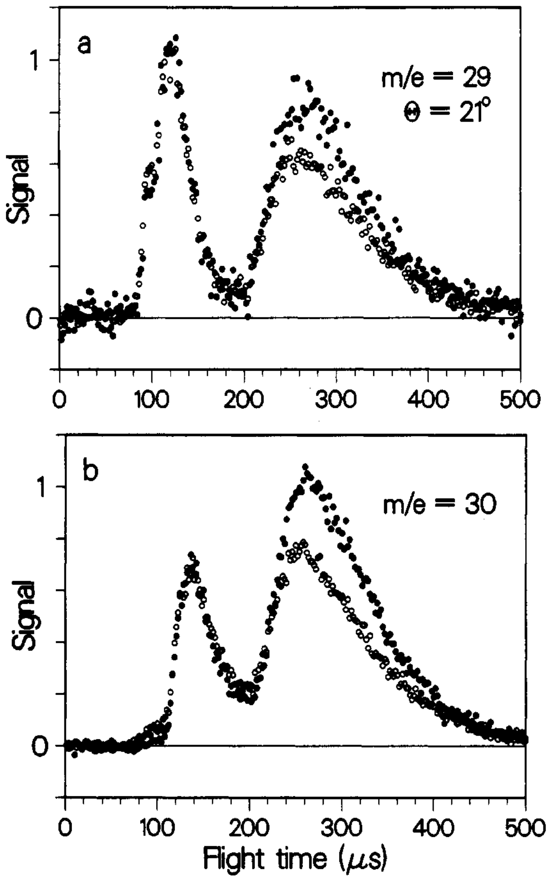

Figure 6. Laser power dependence at 193 nm. TOF distributions at m/e = 29 (a) and 30 (b) with different laser fluences (solid circles ~50 mJ/cm^2, empty circles ~500 mJ/cm^2).

the ionization cross sections and the mass spectra of CH_3ONO and CH_3O, the signal intensities of the TOF distribution measured at $m/e = 29$ can be used to extract an approximate branching ratio for the formation of these species. The appropriate procedure has been described by Krajnovich et al.[30] The ionization cross sections of CH_3ONO and CH_3O were estimated from the relationship[31] $\sigma_{ion} = 36 \times \alpha^{1/2} - 18$, where σ_{ion} is the maximum ionization cross section in units of Å^2 and α is the polarizability in Å^3. At the electron energy used in our experiments (~100 eV) the ionization cross section should be close to the maximum value. The molecular polarizability is approximated by the sum of the atomic polarizabilities, which are found in the literature,[32] and the ion cracking pattern of CH_3ONO was measured as mentioned above, whereas that of the CH_3O radical was derived from the results of a separate experiment on the photodissociation of CH_3OOH.[33] From these measurements, the relative intensities of CHO^+ in the mass spectra of CH_3ONO and CH_3O were found to be 0.15 ± 0.05 and 0.6 ± 0.2, respectively. Recalling that in the TOF spectrum at $m/e = 29$ the peaks A and B are due to CH_3O from reaction I and peak C to CH_3ONO from reaction II, we have adopted the above-mentioned ion fragmentation ratios to correct the apparent weighting factors derived from the TOF simulations. In this manner, we calculated the relative photodissociation yields of reactions I and II to be 0.7 and 0.3, respectively. Moreover, in the case of reaction I, the branching ratio between the decay modes giving rise to peaks A and B is approximately 0.16:0.84.

III.4. Laser Fluence Dependence. To assess the importance of photoinduced secondary reactions, a series of experiments was carried out with attenuated laser power. Figure 6a shows the TOF spectra at $m/e = 29$ recorded with a laser fluence of 50 and 500 mJ/cm^2. While the absolute intensity of the photofragment signal increases as a function of the laser fluence, the *relative* intensity of the TOF component C, which has above been assigned to CH_3ONO produced in reaction II, is found to *decrease* in comparison with the main peak B. This behavior is consistent with the expected[34] depletion of CH_3ONO caused by the secondary photodissociation process

$$CH_3ONO \rightarrow CH_3O + NO \qquad (5)$$

Since the UV absorption cross section of CH_3ONO at 193 nm is about 1 order of magnitude smaller than in methyl nitrate,[34] the secondary photodissociation is almost completely suppressed at the lower laser fluence. The relative intensity of peak A, however, shows a slight *increase* at higher fluence. Again, this behavior can be ascribed to reaction 5. From our previous investigation of the 193-nm photodissociation of CH_3ONO[35] we estimate that the resulting CH_3O fragments should yield a TOF signal at ~90 μs. Since this coincides with the flight time of the fastest primary CH_3O fragments from methyl nitrate, the secondary photodissociation process (5) gives rise to an increase of the signal component A.

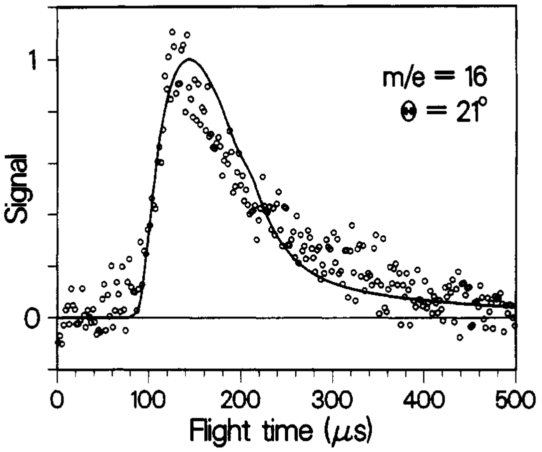

Figure 7. Photodissociation of CH_3ONO_2 at 193 nm. TOF distributions measured at $m/e = 16$ with Θ = 21°.

Reaction 5 can also account for the power dependence observed in the TOF spectrum at $m/e = 30$ shown in Figure 6b. Like their CH_3O partners, the NO fragments formed in this process are expected to have a flight time of approximately 90 μs, where a new signal does indeed appear if the laser fluence is increased. However, part of this signal could also stem from the secondary photolysis of NO_2. (While the absorption cross section at 193 nm is 3–4 times lower in NO_2 than in CH_3ONO, the former species is produced with a yield of ~70%; see above.) Since the translational energy release of the NO_2 photodissociation at 193 nm is not known and since further signal contributions at m/e = 30 are expected from the unimolecular decay of hot NO_2 molecules,[36] no attempt was made to obtain a complete TOF simulation at this mass.

In closing this section, we briefly address the TOF spectrum measured at $m/e = 16$ displayed in Figure 7. The signal, consisting of a single, rather broad peak extending from about 100–400 μs, is predominantly due to the oxygen atoms formed in the primary process II. The solid line in Figure 7 was calculated with the $P(E_T)$ derived from the TOF data at $m/e = 60$ (see Figure 4a) which adequately reproduces the signal at $m/e = 16$. Slight deviations from a perfect fit are readily attributed to various additional signals expected at this mass, most notably from the O atoms produced in the dissociation of hot NO_2 but also from the formation of O^+ daughter ions of the oxygen-containing dissociation products.

III.5. Photodissociation at 248 nm. The TOF spectrum at $m/e = 29$ (CHO^+) recorded with Θ = 21° is shown in Figure 8a. It consists of a single peak which is assigned to CH_3O fragments created in reaction I. The solid line in Figure 8a was calculated with the best-fitting $P(E_T)$ distribution, which in turn is reproduced

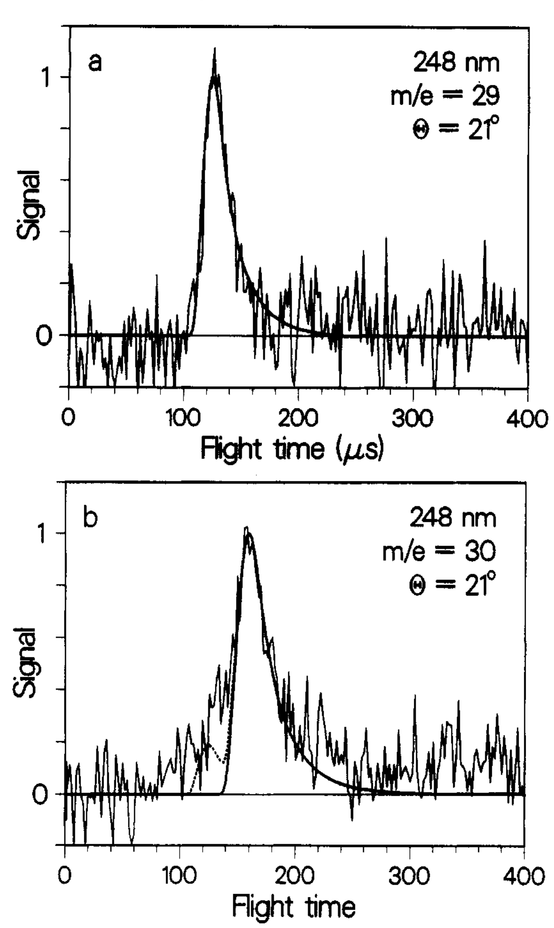

Figure 8. Photodissociation of CH_3ONO_2 at 248 nm. TOF distributions measured at m/e = 29 (a) and 30 (b) with Θ = 21°. The solid line, representing the best fit, was calculated with the $P(E_T)$ distribution shown in Figure 9. The dashed line in (b) is the result of a calculation assuming that the signal at m/e = 30 stems from both the CH_2O^+ (25%) and NO^+ (75%) ions of the CH_3O and NO_2 neutral fragments.

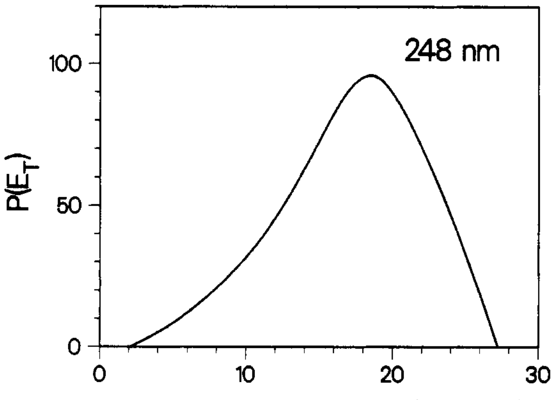

Figure 9. Center-of mass translational energy distribution $P(E_T)$ of the fragments from the photodissociation of CH_3ONO_2 at 248 nm.

in Figure 9. Because the absorption cross section at 248 nm is almost 3 orders of magnitude smaller than at 193 nm, the NO_2 fragments formed at 248 nm had to be detected at m/e = 30 (NO^+, Figure 8b) where the signal to noise ratio was significantly better than at m/e = 46. The TOF spectrum predicted on the basis of the $P(E_T)$ of Figure 9 accounts for most of the TOF signal at m/e = 30 and thus confirms the assignment to reaction I. The additional signal present at flight times between 80 and 140 μs is attributed to CH_2O^+ formed by electron impact ionization of the CH_3O fragments (dashed curve in Figure 8b) and, furthermore, to NO produced by the secondary photodissociation of NO_2.[37]

No signals that could have been assigned to other primary dissociation processes were observed at 248 nm. In particular, no peak was detected at long flight times (>250 μs), in contrast to the slow component "C" that was found upon photolysis at 193 nm. Therefore, we conclude that reaction I is the only important dissociation pathway after irradiation of CH_3ONO_2 with $\lambda \geq$ 248 nm.

IV. Discussion

Upon photoexcitation at 193 nm methyl nitrate dissociates along three different pathways as evidenced by the TOF signal components A, B, and C. Components A and B are *both* associated with the formation of CH_3O and NO_2 (reaction I). For clarity, the two reaction pathways will henceforth be denoted by (IA) and (IB). Signal component C is due to the formation of CH_3ONO and O (reaction II). Before discussing the details of each process, some remarks about their relative importance are in order. The observation of reaction I as the dominant dissociation channel (70%) was not unexpected since it involves the simple fission of the weakest bond in the parent molecule (D_0^{I} = 41 kcal/mol; see Figure 1).[7,8] Reaction II, on the other hand, requires the cleavage of the much stronger N–O bond (D_0^{II} = 118 kcal/mol; see Figure 1 and discussion below). The 30% yield of this reaction is also remarkable in view of the fact that the energetically more favorable process leading to $CH_3 + NO_3$ (reaction 3, with a dissociation energy of 83 kcal/mol; see Figure 1) does not occur. These findings imply a selective photodissociation mechanism for which the electronic transition is localized on the NO_2 group and the internal energy is effectively retained within this moiety during the dissociation process. The occurrence of reaction 3 would require a transfer of the excitation to the CH_3O group, but this appears to be prevented by the weak and easily broken central O–N bond.

A local excitation of the NO_2 group is supported by a series of semiempirical CNDO/s-CI calculations previously carried out by Harris.[6] From a comparison of several molecules containing the NO_2 group, Harris concluded that the electronic transition observed in these compounds around 6.5 eV (~190 nm) is due to excitation of the 1 $^1B_2$ ($\pi_0\pi^*$) state. (In the case of CH_3ONO_2 the nitro group is considered to have local C_{2v} symmetry.) Accordingly, the electronic transition moment μ is oriented parallel to the line connecting the two terminal O atoms. The angular distribution of the photofragments from reaction II is consistent with the spectral assignment by Harris.[6] If the oxygen atom is expelled along the direction r of the original N–O bond of the parent (see insert of Figure 1), the internal recoil angle between μ and r is estimated to be χ = 25° from the equilibrium structure of methyl nitrate in the electronic ground state.[38] This angle causes a "geometrical" reduction[39] of the maximal anisotropy parameter β = 2 to β = 1.45. The experimentally determined β = 1.2 is thus close to the limiting value for instantaneous dissociation. More specifically, based on a rotational frequency $\omega_{rot} = 2.5 \times 10^{11}$ s^{-1} derived from the rotational constant I_c = 147 amu Å^2 of CH_3ONO_2,[38] the formation of CH_3ONO + O is predicted to take place on a time scale <1 ps.

The translational energy distribution of reaction II ranges from 0 to ~20 kcal/mol with an average of 6 kcal/mol (see Figure 4a and Table I). For a given electronic state of the O atom, the $P(E_T)$ distribution directly reflects the internal energy distribution of the CH_3ONO fragments according to the energy balance

$$E_{CH_3ONO} = E_{avl} - E_T \qquad (6)$$

where the available energy has been defined in eq 4. If the oxygen atom were formed in the ground state $O(^3P)$, the available energy E_{avl} = 75 kcal/mol would imply that E_{CH_3ONO} is between 55 and 75 kcal/mol, i.e., all the CH_3ONO fragments formed with a partner $O(^3P)$ would have an internal energy well above the dissociation threshold of 42 kcal/mol.[40] However, since the $P(E_T)$ of reaction II was obtained from the TOF spectra of *undissociated* CH_3ONO fragments, we are forced to conclude that the oxygen atoms are created in the electronically excited state ^1D. Consequently, the endothermicity of reaction II has to be adjusted from 73 to 118 kcal/mol while the concomitant reduction of E_{avl} from 75 to 30 kcal/mol (see Table I) confines the range of internal energies of methyl nitrite to 10–30 kcal/mol. These results are consistent with our observation of stable CH_3ONO and, moreover, the formation of $O(^1D)$ is a spin-allowed process, in contrast to the reaction with the $O(^3P)$ product. A low efficiency of the energetically favorable but spin-forbidden formation of triplet oxygen has been observed in other molecules without heavy atoms, e.g., in the case of the N_2O photolysis at 193 nm.[41]

In addressing reaction I we note the bimodal shape of the translational energy distribution and the different anisotropy parameters of the two $P(E_T)$ components which suggest the presence of two distinct mechanisms for the formation of $CH_3O + NO_2$. Dissociation pathway IA produces relatively fast ($\langle E_T \rangle = 41$ kcal/mol) fragments with an anisotropic recoil distribution $\beta = 0.9$, whereas pathway IB produces photofragments with less translational energy ($\langle E_T \rangle = 19$ kcal/mol) and an isotropic recoil distribution. While no definitive assignment of the two mechanisms is possible with the presently available data, it is noted that the presence of two competing dissociation pathways was also found for the photofragmentation of nitrosyl chloride (ClNO)[15,43] and nitromethane (CH_3NO_2).[42] The photolysis of ClNO at 193 nm produces Cl and NO fragments with a bimodal $P(E_T)$ distribution, the two components of which have significantly different β parameters.[15] This behavior was attributed to the simultaneous excitation of two neighboring potential energy surfaces that are correlated with the formation of Cl atoms in the ground and spin–orbit excited states, respectively.[15,43] The 193-nm photodissociation of CH_3NO_2 is particularly interesting for comparison with CH_3ONO_2. Butler et al.[42] found in a PTS study that $CH_3 + NO_2$ are formed with a bimodal recoil distribution. The faster and predominant component was assigned to the formation of NO_2 in the $\tilde{B}$ ($^2B_1$) excited state, as based on the measured fluorescence emission spectrum, whereas the slower component was assigned tentatively to the ground state of NO_2 formed after internal conversion of CH_3NO_2 to the electronic ground state.[42] The negative recoil anisotropy of the main component is consistent with the excitation of the $B_2 \leftarrow A_1$ transition of CH_3NO_2, in analogy with our findings for reaction II of CH_3ONO_2 (see above).

Returning now to our experimental results, we can conclude that the decay process IA of CH_3ONO_2 *cannot* be induced by the $B_2 \leftarrow A_1$ electronic transition: even if we allow for a considerable deviation of the recoil direction from the orientation of the breaking $CH_3O–NO_2$ bond, the photofragments would have a negative β value. Within the local C_{2v} symmetry of the ONO_2 group the photofragments $CH_3O + NO_2$ with positive β, i.e., from the decay mode IA, must originate from an $A_1 \leftarrow A_1$ excitation with a transition moment parallel to the C_2 symmetry axis. The isotropic recoil of reaction IB, on the other hand, precludes an immediate conclusion about the orientation of μ and thus on the electronic states involved in the photodissociation. However, a loss of anisotropy for purely geometric reasons would require a transition moment oriented at an angle $\chi \sim 55°$ with respect to the $CH_3O–NO_2$ bond. This is not expected to be the case under the local C_{2v} symmetry. Therefore, at least part of the anisotropy loss in process IB is due to the lifetime of the excited state which, together with the small release of kinetic energy, indicates a predissociation of either the A_1 or B_2 excited state of methyl nitrate.

The secondary decomposition of the NO_2 fragment provides further information on the partitioning of the available energy after the primary dissociation step. The *total* internal energy of the $CH_3O + NO_2$ fragment pairs is directly obtained from the measured kinetic energy E_T according to

$$E_{int} = E_{avl} - E_T \qquad (7)$$

with $E_{avl} = 107$ kcal/mol (see Table I). Dissociation of NO_2 requires a minimum energy of 72 kcal/mol[29] and thus can occur only if the translational energy is less than 35 kcal/mol. Our observation that NO_2 undergoes efficient secondary dissociation at kinetic energies as high as 30 kcal/mol (see Figure 4b) shows that most of the internal energy released in the primary decay mode IB is channeled into, or retained within, the NO_2 fragment.

In contrast to the complex photodissociation of CH_3ONO_2 at 193 nm, the photolysis at 248 nm is much simpler. Despite an absorption cross section 400 times smaller than at 193 nm and, therefore, a correspondingly smaller signal-to-noise ratio, our measurements clearly show that reaction I is the only important primary dissociation process at 248 nm; no evidence was found for the formation of $CH_3 + NO_3$ or $CH_3ONO + O$. Obviously, the latter reaction would only be accessible if the oxygen atom were created in the ground electronic state $O(^3P)$, a process which has been claimed for the photolysis of ethyl nitrate.[22] In view of an irradiation wavelength of only 313 nm, it seems likely that the formation of $CH_3CH_2ONO + O(^3P)$ occurs via excitation of a triplet state in the parent molecule. On the other hand, the photolysis at 248 nm gives access to the lowest excited singlet state, most likely via a $\pi^* \leftarrow n$ transition of the NO_2 group.[6]

The translational energy distribution of the $CH_3O + NO_2$ fragments produced at 248 nm (see Figure 9) spans the range between 2 and 27 kcal/mol, with an average of 17 kcal/mol or 23% of the available energy. This rather low kinetic energy release suggests an indirect dissociation mechanism, maybe through internal conversion to the electronic ground state. Since the total internal energy of the fragment pairs is between 47 and 72 kcal/mol, we conclude that the NO_2 fragment does not possess sufficient energy to undergo unimolecular decomposition.

After submission of this paper, we were made aware of very recent work on the photolysis of HNO_3, a molecule closely related to methyl nitrate. Ravishankara and co-workers[44] and, more recently, Nesbitt and co-workers,[45] have carried out careful measurements of the product yields of OH and O atoms. From their results the authors inferred that in the 193-nm photolysis of HNO_3 an additional channel besides $HNO_3 \rightarrow OH + NO_2$ must be operative, most probably the one leading to $O + HONO$. We have also investigated the photolysis of HNO_3 at 193 nm by means of the PTS technique[46] and have determined the relative importance of the $O + HONO$ channel to be ~40%.

V. Conclusion

In a cold molecular beam the photodissociation of methyl nitrate at 193 nm was found to proceed according to the processes

$$CH_3ONO_2 \rightarrow CH_3O(E^A) + NO_2(E'^A) \qquad (IA)$$

$$\rightarrow CH_3O(E^B) + NO_2(E'^B) \qquad (IB)$$

$$\rightarrow CH_3ONO + O(^1D) \qquad (II)$$

With a yield of about 70%, reaction I involves the fission of the weakest bond $CH_3O–NO_2$ ($D_0^I = 41$ kcal/mol). The fragments emerging from this reaction show a bimodal translational energy distribution with $\langle E_T^A \rangle = 41$ kcal/mol ($\langle E_{int}^A \rangle = 66$ kcal/mol) and $\beta^A = 0.9$ for channel IA and $\langle E_T^B \rangle = 19$ kcal/mol ($\langle E_{int}^B \rangle = 88$ kcal/mol) and $\beta^B = 0$ for channel IB. The majority of the NO_2 fragments of the latter process possess sufficient internal energy to undergo secondary dissociation to $NO + O(^3P)$.

The unexpected high efficiency of fragmentation process II, which results from the rupture of the much stronger N–O bond (D_0^{II} = 118 kcal/mol), creates methyl nitrite, CH_3ONO, and electronically excited oxygen atoms O(^{1}D). This decay path has been established from direct measurements of the fragment recoil distribution with $\langle E_T \rangle$ = 6 kcal/mol and β = 1.2.

The selective fission of the strong N–O bond in reaction II and the absence of the fission of the weaker CH_3–ONO_2 bond (D_0 = 83 kcal/mol) suggests an initial localization of the excitation on the NO_2 moiety in the parent molecule and a retention of the excitation energy within this group during the necessarily fast dissociation process II.

For photodissociation at 248 nm only reaction I with a single-peaked fragment translational energy distribution was observed. At this excitation energy the dissociation path II with O(^{1}D) formation is energetically not accessible whereas the same process with the feasible, but spin-forbidden, production of O(^{3}P) fragments (E_{avl} = 75 kcal/mol) was found not to be operative.

Acknowledgment. Support by the Schweizerischer Nationalfonds zur Förderung der wissenschaftlichen Forschung and by the Alfred Werner Legat is gratefully acknowledged. We thank Mr. R. Pfister for the synthesis of methyl nitrate and Dr. P. Willmott for critically reading the manuscript.

References and Notes

(1) Leighton, P. A. *The Photochemistry of Air Pollution*; Academic: New York, 1961.

(2) Crutzen, P. J. *Annu. Rev. Earth Planet. Sci.* **1979**, *7*, 443.

(3) Roberts, J. M.; Fajer, R. W. *Environ. Sci. Technol.* **1989**, *23*, 945.

(4) Atlas, E.; Schauffler, S. Presented at the American Geophysical Union Fall Meeting, San Francisco, CA, Dec 1988.

(5) Taylor, W. D.; Allston, T. D.; Moscato, M. J.; Fazekas, G. B.; Kozlowski, R.; Takacs, G. A. *Int. J. Chem. Kinet.* **1980**, *12*, 231.

(6) Harris, L. E. *J. Chem. Phys.* **1973**, *58*, 5615.

(7) Appin, A. O.; Chariton, J. *Acta Physicochem. U.S.S.R.* **1936**, *5*, 655.

(8) Gray, P.; Rogers, G. T. *Trans. Faraday Soc.* **1954**, *50*, 28.

(9) Busch, G. E.; Mahoney, R. T.; Morse, R. I.; Wilson, K. R. *J. Chem. Phys.* **1969**, *51*, 449.

(10) Wodkte, A. M.; Lee, Y. T. In *Molecular Photodissociation Dynamics*; Ashfold, M. N. R., Baggott, J. E., Eds.; Royal Society of Chemistry: London, 1987.

(11) Ashfold, M. N. R.; Lambert, I. R.; Mordaunt, D. H.; Morley, G. P.; Western, C. M. *J. Phys. Chem.* **1992**, *96*, 2938.

(12) Haas, B.-M.; Minton, T. K.; Felder, P.; Huber, J. R. *J. Phys. Chem.* **1991**, *95*, 5149.

(13) Baum, G.; Effenhauser, C. S.; Felder, P.; Huber, J. R. *J. Phys. Chem.* **1992**, *96*, 756.

(14) Felder, P.; Wannenmacher, E. A. J.; Wiedmer, I.; Huber, J. R. *J. Phys. Chem.* **1992**, *96*, 4470.

(15) Haas, B.-M.; Felder, P.; Huber, J. R. *Chem. Phys. Lett.* **1991**, *180*, 293.

(16) Jackson, W. M.; Anex, D. S.; Continetti, R. E.; Balko, B. A.; Lee, Y. T. *J. Chem. Phys.* **1991**, *95*, 7327.

(17) Keller, J. S.; Kash, P. W.; Jensen, E.; Butler, L. J. *J. Chem. Phys.* **1992**, *96*, 4324.

(18) Minton, T. K.; Nelson, C. M.; Moore, T. A.; Okumura, M. *Science* **1992**, *258*, 1342.

(19) *CRC Handbook of Chemistry and Physics*, 73rd ed.; Weast, R. C., Ed.; CRC Press, Inc.: Boca Raton, FL, 1992.

(20) JANAF Thermochemical Tables, *J. Phys. Chem. Ref. Data* **1985**, *14*, Suppl. 1.

(21) Davis, H. F.; Kim, B.; Johnston, H. S.; Lee, Y. T. *J. Phys. Chem.* **1993**, *97*, 2172 and references therein.

(22) Rebbert, R. E. *J. Phys. Chem.* **1963**, *67*, 1923.

(23) Wayne, R. P. *Chemistry of Atmospheres*, 2nd ed.; Oxford Science Publications: Oxford, 1991.

(24) Felder, P. *Chem. Phys.* **1990**, *143*, 141.

(25) *Organic Synthesis*; Blatt, A. H., Ed.; Wiley: New York, 1943; Collect. Vol. II.

(26) Minton, T. K.; Felder, P.; Brudzynski, R. J.; Lee, Y. T. *J. Chem. Phys.* **1984**, *81*, 1759.

(27) Sparks, R. K.; Shobatake, K.; Carlson, L. R.; Lee, Y. T. *J. Chem. Phys.* **1981**, *75*, 3838.

(28) Zare, R. N. *Mol. Photochem.* **1972**, *4*, 1.

(29) Robra, U.; Zacharias, H.; Welge, K. H. *Z. Phys. D* **1990**, *16*, 175.

(30) Krajnovich, D.; Huisken, F.; Zhang, Z.; Shen, Y. R.; Lee, Y. T. *J. Chem. Phys.* **1982**, *77*, 5977.

(31) Center, R. E.; Mandl, A. *J. Chem. Phys.* **1972**, *57*, 4104.

(32) Miller, T. M.; Bederson, B. *Adv. At. Mol. Phys.* **1977**, *13*, 1.

(33) Thelen, M. A.; Felder, P.; Huber, J. R., to be published.

(34) Keller, B. A.; Felder, P.; Huber, J. R. *J. Phys. Chem.* **1987**, *91*, 1114.

(35) Felder, P.; Keller, B. A.; Huber, J. R. *Z. Phys. D* **1987**, *6*, 185.

(36) Troe, J. *Ber. Bunsen-Ges. Phys. Chem.* **1969**, *73*, 144.

(37) McFarlane, J.; Polanyi, J. C.; Shapter, J. G. *J. Photochem. Photobiol. A: Chem.* **1991**, *58*, 139.

(38) Cox, A. P.; Waring, S. *Trans. Faraday Soc.* **1971**, *67*, 3441.

(39) Yang, S.; Bersohn, R. *J. Chem. Phys.* **1974**, *61*, 4400.

(40) Batt, L.; Christie, K.; Milne, R. T.; Summers, A. J. *Int. J. Chem. Kinet.* **1974**, *6*, 877.

(41) Felder, P.; Haas, B.-M.; Huber, J. R. *Chem. Phys. Lett.* **1991**, *186*, 177.

(42) Butler, L. J.; Krajnovich, D.; Lee, Y. T.; Ondrey, G.; Bersohn, R. *J. Chem. Phys.* **1983**, *79*, 1708.

(43) Kim, H. L.; Mo, Y.; Matsumi, Y.; Kawasaki, M. *Bull. Korean Chem. Soc.* **1992**, *13*, 162.

(44) Turnipseed, A. A.; Vaghjiani, G. L.; Thompson, J. E.; Ravishankara, A. R. *J. Chem. Phys.* **1992**, *96*, 5887.

(45) Schiffman, A.; Nelson, Jr. D. D.; Nesbitt, D. J. *J. Chem. Phys.* **1993**, *98*, 6935.

(46) Felder, P.; Yang, X.; Huber, J. R., to be published.